

Room-temperature, continuous wave lasing in planar microcavities with quantum dots

Andrey Babichev,^{1,*} Mikhail Bobrov,¹ Alexey Vasil'ev,¹ Sergey Blokhin,¹ Nikolay Maleev,¹ Ivan Makhov,² Natalia Kryzhanovskaya,² Leonid Karachinsky,³ Innokenty Novikov,³ and Anton Egorov³

¹Ioffe Institute, Saint Petersburg, Russia

²HSE University, Saint Petersburg, Russia

³TMO University, Saint Petersburg, Russia

*a.babichev@mail.ioffe.ru

Abstract

High-quality planar cavities with low-absorption mirrors based on $\text{Al}_{0.2}\text{Ga}_{0.8}\text{As}/\text{Al}_{0.9}\text{Ga}_{0.1}\text{As}$ layers demonstrate continuous wave lasing at a wavelength of 957 nm. At 300 K, the threshold power density and quality-factor at threshold are (11.4 ± 0.7) kW/cm² and (5070 ± 160) . Increasing the pumping level above two thresholds results in an enlargement in the quality-factor to at least 19000. Efficient lateral heat dissipation in the planar semiconductor microcavity is confirmed by a low mode-energy shift, which is 660 μeV at two lasing thresholds.

Active regions based on quantum dots (QDs) have demonstrated their effectiveness in the fabrication of microdisk[1], dual-state lasers[2], single-photon sources[3], and vertical microcavity lasers[4–9].

High-speed spin-lasers[10] based on bimodal QDs micropillar cavities have recently been demonstrated. Compared with birefringent vertical-cavity surface-emitting lasers (VCSELs)[10] and optically pumped microlasers[11], micropillar cavity lasers with a large quality-factor (Q-factor) are of interest for quantum nanophotonics[12] and neuromorphic computing (NC)[12,13]. Reservoir computing (RC) is one of the NC schemes. The RC concept, based on diffraction-coupled laser arrays, has been presented for both VCSELs[14–17] and optically pumped microlasers[12]. An optical reservoir computer based on current-injected VCSELs (24 physical nodes) operating at room-temperature has been implemented[14].

The prospects for using optically pumped micropillar cavities as a RC are determined by the small pitch on the substrate[12] and the possibility of operating at room temperature[18]. To achieve a high Q-factor, an optimized vertical deep ($\sim 7\text{--}10$ μm) dry etching process is required.

To mitigate deep etching of micropillar cavities, a concept of vertical photonic-defect hybrid microcavities with embedded QDs was invented[8]. Due to the quasi-planar geometry, this concept excludes non-radiative surface recombination at the sidewalls, which is crucial when using quantum wells (QWs)-based active regions[12].

Photonic-defect microcavities[7,8] include a semiconductor bottom mirror, a GaAs cavity with embedded QDs, and a dielectric output mirror deposited on a partially etched microcavity mesa. A micro-curved dielectric mirror, which was also used in the fabrication of blue GaN-based VCSELs[19], functions as a photonic-defect[7,8].

To exclude the second epitaxy process, a dielectric top mirror was used[20]. Compared to the process of epitaxial regrowth of mesa (buried mesa)[21–25], it can be easily deposited/sputtered. Furthermore, the large refractive index contrast of dielectrics allows for a reduction in the number of mirror pairs. The bottom mirror included GaAs/ $\text{Al}_{0.9}\text{Ga}_{0.1}\text{As}$ layers, which are characterized by a larger refractive index contrast, but have significantly greater loss at the pump wavelength compared to $\text{Al}_{0.2}\text{Ga}_{0.8}\text{As}/\text{Al}_{0.9}\text{Ga}_{0.1}\text{As}$ mirrors. Compared to micropillar cavities, the active region layers are not etched, and photonic-defect microcavities based on QWs are also possible. Furthermore, the quasi-planar microcavities concept provides efficient lateral heat dissipation[7,8].

The discussed advantages of photonic-defects cavities (absence of non-radiative surface recombination and efficient lateral heat dissipation) are also characteristic of planar cavities. Q-factor simulations were performed for these two types of cavities[7,8]. The transition from planar to quasi-planar (photonic-defect) cavities can positively affect the Q-factor when using a design with a shallow mesa[8]. On the contrary, the use of a deep mesa leads to the opposite effect and deterioration of the Q-factor compared to a planar cavity[8].

In the first experiment for quasi-planar cavities[8], the etch depth was 100 nm, which resulted in a modest increase in the Q-factor from 10500 (non-etched cavity) to 11000 (photonic-defect cavity). The maximum operation temperature was 260 K, and the threshold power density of 512 kW/cm² (16.1 mW)[8]. Increasing the etching depth to 120 nm, as well as the diameter of photonic-defect, allows operating at room temperature. The threshold power density for a 5 μm in diameter photonic-defect cavity was 156 kW/cm² (4.9 mW)[7].

In this Letter, we present the first results of a study of planar vertical microcavities based on $\text{Al}_{0.2}\text{Ga}_{0.8}\text{As}/\text{Al}_{0.9}\text{Ga}_{0.1}\text{As}$ mirrors operating at room temperature. Compared to micropillar and photonic-defect cavities, this concept does not require deep mesa etching and can be implemented in a single epitaxial process, which is important for the practical application of microcavity lasers.

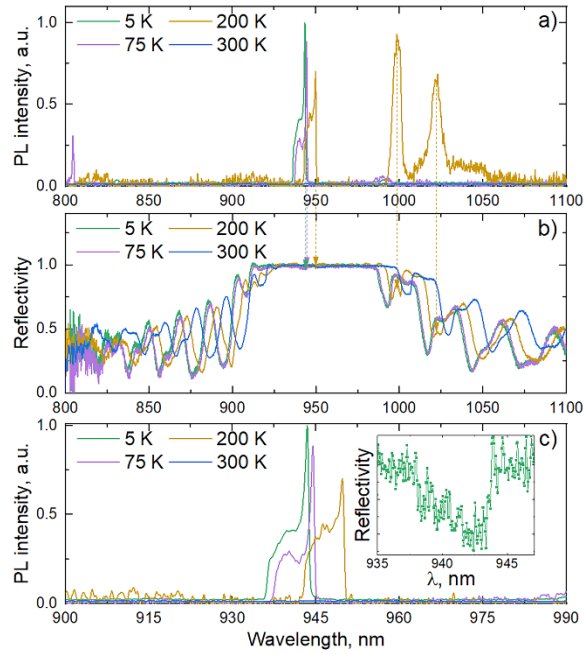


Figure 1. (a) and (c) PL spectra (normalized) of a planar cavity structure with QDs, measured from the surface of the structure; (b) Reflection spectra of a planar cavity structure with QDs, measured from the surface of the structure. The inset in panel (c) shows an enlarged reflection spectrum measured at 5 K.

Molecular-beam epitaxy was used to grow the planar cavity structure. A GaAs cavity with a length of one lambda (see Figure 3, inset) was formed using low-absorption $\text{Al}_{0.2}\text{Ga}_{0.8}\text{As}/\text{Al}_{0.9}\text{Ga}_{0.1}\text{As}$ mirrors (at the pump wavelength)[26]. To fabricate a high-quality semiconductor microcavity structure, the bottom and top mirrors include 37.5 and 32 pairs. The modelled Q-factor of the cold cavity, determined at 300 K, is 82400. Stranski-Krastanow growth method was used to self-assembly of initial InGaAs QDs. 18 To increase the modal gain of the active region, three stacked layers of QDs were used.

For optical characterization, the planar cavity structure was measured by placing in a Cryostat[®] s50 closed-cycle optical cryostat, which provides exceptional thermal and vibrational stability. Optical pumping was performed in continuous wave mode. A Mitutoyo MPlan Apo NIR 20 \times microscope was used to focus the emission on the sample. Surface emission spectra were collected using the same microobjective used for pumping. An Andor Shamrock 500i spectrometer (with a focal length of 500 mm) was used to measure the emission spectra. A back-illuminated silicon CCD detector (Andor iDus 401A) was used for signal detection. The spectrometer was combined with a 1200 lines/mm diffraction grating, providing a resolution of 0.05 nm.

Reflection/spontaneous emission spectra from of the planar cavity structure (see Figure 1) were excited and collected using a microobjective similar to that used in the experiment to study stimulated emission spectra (see Figure 2). Optical pumping was performed at a wavelength of 527 nm. A Mitutoyo MPlan Apo NIR 50 \times objective was used to obtain a 2- μm -diameter spot on the sample. The pump power was 95 μW at temperatures of 5 and 77 K and increased to 700 μW at temperatures of 200 and 300 K.

First, we present the results of photoluminescence (PL) spectra measurements of a planar cavity structure pumped at a wavelength of 527 nm (see Figure 1(a) and (c)). At 5 K, the PL spectrum exhibits a high-intensity peak near 543 nm, the position of which coincides with the position of the dip in the reflectivity stopband (see Fig. 1(b)). An additional low-intensity peak is observed near 990 nm (see Figure 1(a)), which is associated with the position of the fringe in the reflectivity spectrum.

Increasing the temperature to 75 K shifts of the main PL peak to approximately 945 nm (see Figure 1(c)). The main peak also exhibits an additional short-wavelength shoulder (in the range of 937–945 nm), similar to the results at 5 K. This shoulder is associated with absorption in the active region, which also leads to an asymmetric dip in the reflectance spectrum (see Figure 1(c), inset). The emission corresponding to the position of the fringe in the reflection spectrum is demonstrated at a wavelength of 990 nm.

At 200 K, the main PL peak, corresponding to the position of the dip in the reflection spectrum, is located at a wavelength of 950 nm (see Figure 1(c)). Compared to the results obtained at low temperatures (at 5 and 77 K), two emission peaks are observed, corresponding to the position of the fringes in the reflection spectrum (at 998 and 1022 nm, see Figure 1(b)). The reason for this is the increase in the pump power density from 3.0 kW/cm^2 (spectra measured at 5 and 75 K) to 22.3 kW/cm^2 . The intensity of the peaks corresponding to the interference fringes in the reflection spectrum exceeds the intensity of the PL peak associated with the resonance wavelength of the vertical microcavity. This is explained by the smaller temperature shift of the resonance wavelength compared to the temperature shift of the peak from the QDs. A further increase in temperature to 300 K results in the absence of spontaneous emission signal detected through the output mirror at a given pump power density of 22.3 kW/cm^2 .

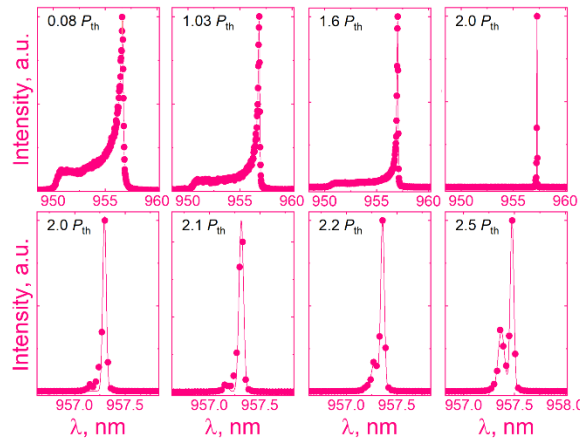


Figure 2. Normalized emission spectra of a planar microcavity structure measured at 300 K. The bottom panels (in the pump power density range 2.0–2.5× P_{th}) correspond to the enlarged scale along the X-axis.

To clarify the reason for the absence of emission at a pump power density twice the threshold pump power density determined at a pump wavelength of 808 nm (see below), it is necessary to estimate the power conversion efficiency (PCE) at both wavelengths. This value is determined by the transmission of the output mirror (T_{mirror}) and the absorption of the active region ($A(\lambda)$)[27].

The absorption coefficient of $Al_{0.2}Ga_{0.8}As$ at 527 nm is 63604 cm^{-1} , which is approximately 570 times larger than that at 808 nm [28]. Absorption within the $Al_{0.9}Ga_{0.1}As$ layers is observed only at the pump wavelengths of 527 nm ($\sim 900 \text{ cm}^{-1}$)[28]. As a result, optical loss in the mirrors are mainly associated with the $Al_{0.2}Ga_{0.8}As$ layers.

Taking into account the absorption coefficients of the mirror layers ($\alpha_{AlGaAs}(\lambda, T)$), the value of T_{mirror} can be estimated using the expression[29] $T_{mirror} = (1 - R(\lambda))\exp(-\alpha_{AlGaAs}(\lambda, T)d_{mirror})$, where $R(\lambda)$ is the reflectivity at the wavelength λ and d_{mirror} is the total thickness of the mirror layers.

The $A(\lambda)$ value is determined according to $A(\lambda) = 1 - \exp(-\alpha_{GaAs}(\lambda, T)d_{AR})$, where α_{GaAs} is the absorption coefficient of the cavity layer (GaAs) and d_{AR} is the cavity thickness[29]. As a result, the use of pumping at short wavelengths leads to an increase in the absorption coefficient of GaAs and, consequently, to an enlarge in the absorption of the active region. The latter value can have a positive effect on the power conversion efficiency. Since the α_{GaAs} value determined at 527 nm is 82844 cm^{-1} [28], which is 7.5 times larger than at 808 nm, the extracted $A(\lambda)$ value increases to 0.82 compared to 0.21 at 808 nm. Despite this positive effect, the contribution of the output mirror transmittance remains dominant in the case of strong absorption in its layers.

The power conversion efficiency extracted at 527 nm is $3.75 \times 10^{-5} \%$, compared to 14.9 % at 808 nm. This is the main factor limiting laser action in planar cavities pumped at 527 nm.

Figure 2 shows the emission spectra measured at 300 K, which corresponds to a pump wavelength of 808 nm. Against the background of spontaneous emission (in the range of 949–957 nm), a superlinear increase in the mode intensity (at $\sim 957 \text{ nm}$) is observed with a raise in the pump power.

It has been previously shown that the pronounced S-shape of the input-output (I-O) curve, along with linewidth narrowing, indicates an underlying laser transition for micropillar[27] and photonic-defect hybrid[7,8] microcavities. Photon autocorrelation studies can be used to provide further evidence for the laser transition[7].

The luminescence line ($\sim 957 \text{ nm}$) at different pump levels was approximated (Gauss line shape fitting[29]). The emission intensity was analyzed by solving the laser rate-equations[11]. The dependence of the pump power density P on the number of photons in the microcavity n is described by the expression[11]: $P(n) = A[n(1+\xi)(1+\beta n)/(1+n) - \xi\beta n]$, where ξ is a scaling factor that takes into account the exciton number of photons at the transparency threshold, β is the spontaneous emission factor and A is the scaling factor.

The result of fitting the I-O characteristic defined using this expression, is shown in Figure 3. The estimated β -factor is $(1.4 \pm 0.05) \times 10^{-3} \%$. The threshold pump density P_{th} is derived from the reduced expression: $P(n) = A(1 + 2\xi + 2\beta \times (1 - \xi)) / 3\beta$ and is equal to $(11.4 \pm 0.7) \text{ kW/cm}^2$. The threshold absorbed power density, determined by multiplying the power conversion efficiency by the threshold power density, is $(1.7 \pm 0.1) \text{ kW/cm}^2$. The Q-factor at threshold is 5070 ± 160 .

Increasing the pump power density to $2.0 \times P_{th}$ leads to a decrease in the linewidth (increase in Q-factor) to 0.05 nm (19000), which is limited by the spectral resolution of the monochromator used. A further increase in the pump power density leads to a gain in the intensity of the additional mode (see Figure 2, at $2.5 \times P_{th}$), which causes a decrease in the intensity of the fundamental mode and an increase in its linewidth (see Figure 3).

To analyze thermal issues, the mode energy shift (ΔE) is commonly analyzed[27], which is shown in Figure 3. Increasing the pump power from $0.1(1.0) \times P_{th}$ to $2.0 \times P_{th}$ results in a redshift of ΔE value by approximately 1.0 (0.66) meV. Raising the pump power from $0.1(1.0)$

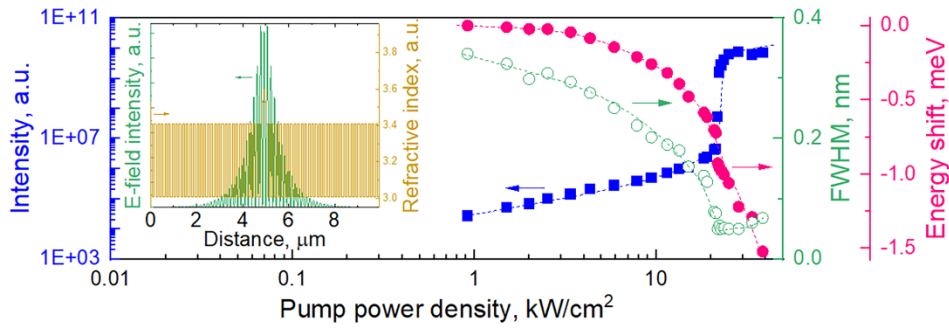


Figure 3. I-O characteristic of a planar microcavity structure (left Y-axis). Linewidth and mode energy shift at different pump power density (left Y-axes). The inset shows the optical field intensity (left Y-axis) and refractive index (right Y-axis) profiles.

to $3.4 \times P_{th}$ results in a mode energy shift of approximately 1.5 meV (1.2 meV). This pump level corresponds to a power density of 38.6 kW/cm^2 .

For comparative analysis, the mode energy shift of micropillar lasers operating at room temperature[18] should be discussed. The lasing threshold for a pillar with a diameter of $5 \text{ } \mu\text{m}$ corresponds to the threshold power density of 6.2 kW/cm^2 . With an increase in the pump power density from $0.1(1.0)$ to $2.0 \times P_{th}$, a mode energy shift of 2.6 (2.3) meV was extracted[18]. Raising the pump power density to $4.0 \times P_{th}$ compared to $0.1(1.0) \times P_{th}$ leads to a shift in the mode energy by 5.2 (4.6) meV. This pumping level corresponds to a pump power density of 24.4 kW/cm^2 . As a result, compared to micropillars, the use of planar cavities allows for a significant reduction in the mode energy shift (thermal issues).

In conclusion, compared with hybrid photonic-defect cavities that used a non-absorbing dielectric output mirror[7], the use of a low-absorption output mirror (based on $\text{Al}_{0.2}\text{Ga}_{0.8}\text{As}/\text{Al}_{0.9}\text{Ga}_{0.1}\text{As}$ layers) results in additional heating, which was observed in micropillar cavity lasers[7,18]. As a result, the thermal lens effect[30] makes it possible to implement optical confinement in planar cavities based on $\text{Al}_{0.2}\text{Ga}_{0.8}\text{As}/\text{Al}_{0.9}\text{Ga}_{0.1}\text{As}$ mirrors.

In the examined planar cavity, increasing the pump power from 0.1 to $1.0 \times P_{th}$ leads to a mode energy shift of $320 \text{ } \mu\text{eV}$, which corresponds to a wavelength shift of 0.23 nm . Based on the temperature shift of the dip position (0.058 nm/K)[26], the heating with increasing pump power from 0.1 to $1.0 \times P_{th}$ is approximately 4°C . A further raising in the pump power to 2.0 and $3.4 \times P_{th}$ led to heating of approximately 12 and 19°C . Taking into account the temperature shift of the refractive index ($4 \times 10^{-4} \text{ K}^{-1}$),³⁰ increasing the pump level to the lasing threshold provides a lateral refractive index contrast (Δn) of 1.6×10^{-3} . A further raising in the pump power to $3.4 \times P_{th}$ leads to a Δn value of 8×10^{-3} .

It should be noted that planar vertical microcavities have been studied previously. Planar GaAs/AlAs cavities with QWs[31] and QDs[32] have been examined. Due to the use of highly absorbing (at a wavelength of 514 nm) GaAs/AlAs mirrors, lasing in a planar vertical microcavity based on an $\text{In}_{0.14}\text{Ga}_{0.86}\text{As}$ QW was not observed[31]. The use of an opposite pumping scheme (wetting layers, WLs, pumping, at a wavelength of 826 nm), mitigates absorption inside GaAs/AlAs mirror layers. At the same time, due to the small thickness of the WLs, the PCE is less than one percentage,²⁹ which also limits the lasing action in planar GaAs/AlAs cavities with InAs QDs[32].

In summary, a new type of room-temperature microlasers based on high-quality planar semiconductor microcavities is presented. Coherent lasing at room temperature is confirmed by a clear S-shaped I-O characteristic and linewidth narrowing[7]. At 300 K , the threshold power density is approximately twice that of micropillar cavities.¹⁸ The Q-factor at threshold decreases to 5070 compared to 8100 for micropillar cavities[18].

Compared to micropillar lasers[18], the relative mode energy shift when doubling the lasing threshold is 3.5 times smaller. As a result, the use of planar cavities allows for a significant reduction in thermal issues compared to micropillars due to possibility of lateral heat dissipation.

In comparison to quasi-planar (photonic-defect) hybrid cavities[7], the examined planar cavities demonstrate a 14-fold reduction in threshold power density. A similar Q-factor at threshold is extracted (~ 5000)[7].

References

1. A. Zhukov et al., "Fast switching between the ground- and excited-state lasing in a quantum-dot microdisk triggered by sub-pulses," *Optics Letters*, vol. 49, no. 2, p. 330, Jan. 2024, doi: 10.1364/ol.509297.
2. M. Dillane, E. A. Viktorov, and B. Kelleher, "Inhibitory and excitatory integration with a quantum dot laser neuron," *Optics Letters*, vol. 48, no. 1, p. 21, Dec. 2022, doi: 10.1364/ol.475805.

3. C. Jimenez, S. Wijitpatima, S. Reitzenstein, and A. Herkommer, "Numerical analysis of coupling efficiency limits in single-photon sources to fiber systems via idealized lens models," *Optics Letters*, vol. 50, no. 16, p. 5002, Aug. 2025, doi: 10.1364/ol.569479.
4. A. Babichev et al., "Low-Threshold Surface-Emitting Whispering-Gallery Mode Microlasers," *IEEE J. Sel. Top. Quantum Electron.*, vol. 31, no. 2, pp. 1–8, Mar. 2025, doi: 10.1109/jstqe.2024.3503724.
5. A. Babichev et al., "Lasing of Quantum-Dot Micropillar Lasers Under Elevated Temperatures," *IEEE J. Sel. Top. Quantum Electron.*, vol. 31, no. 5, pp. 1–8, Sep. 2025, doi: 10.1109/jstqe.2024.3494245.
6. I. Limame et al., "Diameter-dependent whispering gallery mode lasing effects in quantum dot micropillar cavities," *Optics Express*, vol. 32, no. 18, p. 31819, Aug. 2024, doi: 10.1364/oe.529679.
7. K. Gaur et al., "Photonic - Defect Cavities as Next - Generation Room - Temperature Microlasers: A Comparative Study with Micropillars," *Laser & Photonics Reviews*, vol. 19, no. 18, May 2025, doi: 10.1002/lpor.202500533.
8. K. Gaur et al., "High- β lasing in photonic-defect semiconductor-dielectric hybrid microresonators with embedded InGaAs quantum dots," *Applied Physics Letters*, vol. 124, no. 4, Jan. 2024, doi: 10.1063/5.0177393.
9. C. Shih et al., "Self - Aligned Photonic Defect Microcavity Lasers with Site - Controlled Quantum Dots," *Laser & Photonics Reviews*, vol. 18, no. 7, Mar. 2024, doi: 10.1002/lpor.202301242.
10. U. Diiankova et al., "Multimode vertical-cavity surface-emitting lasers under spin injection," *APL Photonics*, vol. 10, no. 10, Oct. 2025, doi: 10.1063/5.0286998.
11. N. Heermeier et al., "Spin - Lasing in Bimodal Quantum Dot Micropillar Cavities," *Laser & Photonics Reviews*, vol. 16, no. 4, Feb. 2022, doi: 10.1002/lpor.202100585.
12. T. Heindel, J.-H. Kim, N. Gregersen, A. Rastelli, and S. Reitzenstein, "Quantum dots for photonic quantum information technology," *Advances in Optics and Photonics*, vol. 15, no. 3, p. 613, Aug. 2023, doi: 10.1364/aop.490091.
13. T. Heuser, J. Grose, S. Holzinger, M. M. Sommer, and S. Reitzenstein, "Development of Highly Homogenous Quantum Dot Micropillar Arrays for Optical Reservoir Computing," *IEEE Journal of Selected Topics in Quantum Electronics*, vol. 26, no. 1, pp. 1–9, Jan. 2020, doi: 10.1109/jstqe.2019.2925968.
14. M. Pflüger, D. Brunner, T. Heuser, J. A. Lott, S. Reitzenstein, and I. Fischer, "Experimental reservoir computing with diffractively coupled VCSELs," *Optics Letters*, vol. 49, no. 9, p. 2285, Apr. 2024, doi: 10.1364/ol.518946.
15. T. Heuser, M. Pflüger, I. Fischer, J. A. Lott, D. Brunner, and S. Reitzenstein, "Developing a photonic hardware platform for brain-inspired computing based on 5x5 VCSEL arrays," *Journal of Physics: Photonics*, vol. 2, no. 4, p. 044002, Aug. 2020, doi: 10.1088/2515-7647/aba671.
16. M. Pflüger, D. Brunner, T. Heuser, J. A. Lott, S. Reitzenstein, and I. Fischer, "Injection locking and coupling the emitters of large VCSEL arrays via diffraction in an external cavity," *Optics Express*, vol. 31, no. 5, p. 8704, Feb. 2023, doi: 10.1364/oe.473449.
17. D. Brunner and I. Fischer, "Reconfigurable semiconductor laser networks based on diffractive coupling," *Optics Letters*, vol. 40, no. 16, p. 3854, Aug. 2015, doi: 10.1364/ol.40.003854.
18. A. Babichev et al., "Advanced micropillar cavities: Room-temperature operation of microlasers," *Applied Physics Letters*, vol. 128, no. 5, Feb. 2026, doi: 10.1063/5.0311163.
19. H. Nakajima et al., "Single transverse mode operation of GaN-based vertical-cavity surface-emitting laser with monolithically incorporated curved mirror," *Applied Physics Express*, vol. 12, no. 8, p. 084003, Jul. 2019, doi: 10.7567/1882-0786/ab3106.
20. T. Watanabe et al., "Wafer-bonded InP-based vertical-cavity surface-emitting lasers using fast atomic beam-activated Si," *Japanese Journal of Applied Physics*, vol. 65, no. 1, p. 010902, Jan. 2026, doi: 10.35848/1347-4065/ae3129.
21. A. Babichev et al., "Impact of Device Topology on the Performance of High-Speed 1550 nm Wafer-Fused VCSELs," *Photonics*, vol. 10, no. 6, p. 660, Jun. 2023, doi: 10.3390/photonics10060660.
22. S. A. Blokhin et al., "20-Gbps 1300-nm range wafer-fused vertical-cavity surface-emitting lasers with InGaAs/InAlGaAs superlattice-based active region," *Optical Engineering*, vol. 61, no. 09, Sep. 2022, doi: 10.1117/1.oe.61.9.096109.
23. A. Gatto et al., "Multi-Tb/s Transmission Based on DMT-Modulated VCSELs in Metro Networks Assisted by Volterra Equalization," *IEEE Access*, vol. 12, pp. 154294–154309, 2024, doi: 10.1109/access.2024.3484003.
24. A. Babichev et al., "Single-Mode High-Speed 1550 nm Wafer Fused VCSELs for Narrow WDM Systems," *IEEE Photonics Technology Letters*, vol. 35, no. 6, pp. 297–300, Mar. 2023, doi: 10.1109/lpt.2023.3241001.
25. S. Jatta et al., "Bulk-Micromachined VCSEL At 1.55 μm With 76-nm Single-Mode Continuous Tuning Range," *IEEE Photonics Technology Letters*, vol. 21, no. 24, pp. 1822–1824, Dec. 2009, doi: 10.1109/lpt.2009.2034272.
26. A. Babichev, et al., "Quantum-Dot Surface-Emitting Lasers: Micropillar Cavities Grown by Molecular-Beam Epitaxy," *IEEE Journal of Selected Topics in Quantum Electronics*, vol. 32, no. 1, pp. 1–9, Feb. 2026, doi: 10.1109/jstqe.2026.3662809.
27. C.-W. Shih et al., "Low-threshold lasing of optically pumped micropillar lasers with Al_{0.2}Ga_{0.8}As/Al_{0.9}Ga_{0.1}As distributed Bragg reflectors," *Applied Physics Letters*, vol. 122, no. 15, Apr. 2023, doi: 10.1063/5.0143236.
28. D. E. Aspnes, S. M. Kelso, R. A. Logan, and R. Bhat, "Optical properties of Al_xGa_{1-x}As," *Journal of Applied Physics*, vol. 60, no. 2, pp. 754–767, Jul. 1986, doi: 10.1063/1.337426.

29. L. Andreoli et al., "Optical pumping of quantum dot micropillar lasers," *Optics Express*, vol. 29, no. 6, p. 9084, Mar. 2021, doi: 10.1364/oe.417063.
30. M. Brunner, K. Gulden, R. Hövel, M. Moser, and M. Illegems, "Thermal lensing effects in small oxide confined vertical-cavity surface-emitting lasers," *Applied Physics Letters*, vol. 76, no. 1, pp. 7–9, Jan. 2000, doi: 10.1063/1.125638.
31. T. Gutbrod et al., "Weak and strong coupling of photons and excitons in photonic dots," *Physical Review B*, vol. 57, no. 16, pp. 9950–9956, Apr. 1998, doi: 10.1103/physrevb.57.9950.
32. J. M. Gérard et al., "Quantum boxes as active probes for photonic microstructures: The pillar microcavity case," *Applied Physics Letters*, vol. 69, no. 4, pp. 449–451, Jul. 1996, doi: 10.1063/1.118135.